# Non-Line-of-Sight 2 x *N* Indoor Optical Camera Communications

NAVID BANI HASSAN[1,*], ZABIH GHASSEMLOOY[1,2,*], STANISLAV ZVANOVEC[3], PENGFEI LUO[4], AND HOA LE-MINH[1]

[1] Optical Communications Research Group, Northumbria University, Newcastle-upon-Tyne, NE1 8ST, UK
[2] QIEM, Chinese Academy of Sciences, Fujian, China
[3] Department of Electromagnetic Field, Czech Technical University in Prague, Technicka 2, 16627 Prague, Czech Republic
[4] Research Department of HiSilicon, Huawei Technologies Co., Ltd, Beijing 100085, P. R. China
[*] Corresponding authors: navid.hassan@northumbria.ac.uk, z.ghassemlooy@northumbria.ac.uk

Compiled November 27, 2017

**We propose, for the first time, a novel non-line-of-sight 2 × *N* indoor optical camera communication system, where *N* is the number of pixels in the camera with a unique packet structure and a detection methodology for extracting the data from the recorded video streams. A comprehensive theoretical model for the proposed system is presented. The proposed system is experimentally investigated and the measured results show that higher ISO levels and exposure times led to reduced transmit power level by 3 dB for every doubling of the exposure time and ISO at a bit error rate of $10^{-3}$. It is also shown that when the overlapping area of two interfering transmitters is larger than approximately 30% of the footprints, the data cannot be recovered.** 

***OCIS codes:*** *(230.3670) Light-emitting diodes; (040.1490) Cameras; (120.5700) Reflection; (060.0060) Fiber optics and optical communications.*

http://dx.doi.org/10.1364/ao.XX.XXXXXX

## 1. INTRODUCTION

The wide spread use of light emitting diodes (LEDs) in indoor and outdoor environments has opened up growing research activities in the emerging field of visible light communications (VLC), see [1] and the references within. Line of sight (LOS) VLC systems employing LEDs, and standard photodiodes (PDs) have been adopted in many applications offering high data rates $R_b$ over a short transmission span (1 to 2 m). However, LOS based links suffer from shadowing and limited user mobility [1]. Both mobility and shadowing can be addressed by adopting (i) multi-array transmitters (Txs) and receivers (Rxs) (i.e., increased complexity); and (ii) the diffuse system but at the cost of reduced $R_b$, see [1, 2] and the references within.

The wide spread use of smart devices equipped with LED based screen lighting and flashlight as well as front and rear high-quality cameras offer the opportunity to establish VLC links, where the flashlight and the camera can be used as a transceiver without the need for additional hardware. The optical camera communications (OCC) offer new possibilities for the use of VLC systems in a number of applications including display based transmission, device to device communications (D2DC) - as part of the Internet of things, vehicular communications where the camera based Rx will offer multiple functionalities including vision, data transmission, localization and range measurement [1, 3–6]. In contrast to the single PD-based VLC systems, a camera based Rx in OCC, which is composed of an imaging lens and image sensor (IS) has many unique features incluing a wide field of view (FoV) due to the PD array, as well as spatial and wavelength separation of light beams [7].

One of the main challenges in OCC is the low frame rate of the camera, hence low data rates of OCC. However, due to the development of the complementary metal-oxide semiconductor (CMOS) image sensor technology, the quality of the captured videos with digital cameras has improved significantly in recent years. Up-to-date smartphone cameras are capable of recording video streams up to 960 frames per second (fps) at 720p resolution [8]. Moreover, similar to other MIMO systems the complexity of the receiver is high. The other challenge is the detection of Tx, since it covers only part of the captured image, and a number of solutions have been proposed such as frame subtraction in both LOS [9, 10] and non-LOS (NLOS) links [11], block matching [12], and vision-based image processing [13]. Also, tracking a moving object in the video stream is an issue in OCC [11, 14]. Most OCC systems reported are based on the LOS path. However, in scenarios where the Txs are not within the LOS FoV, such as two vehicles approaching a cross-road, vehicles travelling on a motorway, and D2DC, the connection will be via the NLOS paths [11]. In NLOS, the reflected beams normally have

large off-axis projected optical illumination footprints, which can increase the link tolerance to the camera movements. In [5, 15] a rolling shutter camera was used to receive reflected lights in an indoor environment, whereas in [16] OCC demodulation based on detection of high-frequency changes of the LED light reflected from surfaces was reported for localization purposes. Despite the higher bit rate, the link span of rolling shutter-based OCC is severely limited and the bit rate changes with the distance and the size of the optical footprint [15]. Besides, the detection system of rolling shutter based-OCC is highly complex.

To the best of our knowledge, in this paper for the first time, an end-to-end NLOS $2 \times N$ OCC system is proposed, which is based on a combination of successive frame subtraction, mask matching and differential signalling schemes for detection and transmission, respectively. A unique non-standard packet structure is suggested for the proposed system and the detection algorithm is given. We experimentally investigate the system bit error rate (BER) performance, and show that BER is improved by increasing both the ISO and the exposure time $T_{exp}$ of the camera. Since the proposed algorithm utilizes averaging over an area in the image, it radically reduces the impact of noise on the performance of the system. We show that a very low transmitting power of 9 mW is needed to achieve a BER of $10^{-3}$ at a link span of 5 m. Moreover, we investigate the impact of interference of other transmitters on the performance of the link and show that with two transmitters if the overlapping area of the optical footprints is more than 30% of the total footprint of a single transmitter then the signal cannot be fully recovered.

The rest of the paper is organized as follows. In Section II, the system model is presented. In Section III, theoretical analysis and the proposed detection algorithm is introduced. In Section IV, the experimental setup and results are discussed. Finally, Section V concludes the paper.

## 2. SYSTEM MODEL

The schematic block diagram of the proposed $2 \times N$ OCC system is shown in Fig. 1(a). At the Tx, a non-return-to-zero on-off keying (NRZ-OOK) input data stream $d_l$ , where $l = 1, 2$, is applied to the packet generator; the output of which is differentially encoded with $x_{k,l} = x_{k-1,l} \oplus b_{k,l}$ prior to intensity modulation of LEDs. $\oplus$ represents the modulo-2 addition, $b_{k,l}$ is the output of packet generator block and $x_{k,l}$ is the output of differential signalling block. Note that, the initial state of modulo-2 addition $x_0$ is assumed to be 0, and $R_b$ is set to half of the camera frame rate $f_r$. Two rectangular boxes ($RB_1$, $RB_2$) located in front of LEDs are used to project a desired illumination patterns on to the floor, see Fig. 1(b), create a beam angle of $\phi_l = 2 \times \tan^{-1}\left(\frac{w_{RB,l}}{2H_{RB,l}}\right)$ for each Tx, where $w_{RB,l}$ and $H_{RB,l}$ represent the width and height of boxes, respectively, and $l = 1, 2$. Fig. 2 illustrates a proposed packet structure, which is composed of *start* (11-bit), *mask* (*M*-bit), where $M$ is the number of Txs, and *data* (1000-bit) as in [17]. Note that, a common start for both Txs can be used since LEDs are synchronized. The mask is used to determine the position of the reflected light beams from the floor, and its length depends on the number of Txs. Here, we have used two sequences of 0, 1 and 0, 0 for $Tx_1$ and $Tx_2$, respectively, which also represent the Tx's identity.

At the Rx a typical digital camera is used to capture the reflected lights from the floor. Each video file is composed of 10 packets of 1013-bit long, which corresponds to a 5.8 minutes video stream. The output video stream of the camera is processed in Matlab in order to recover $d_l$. In most cameras, three

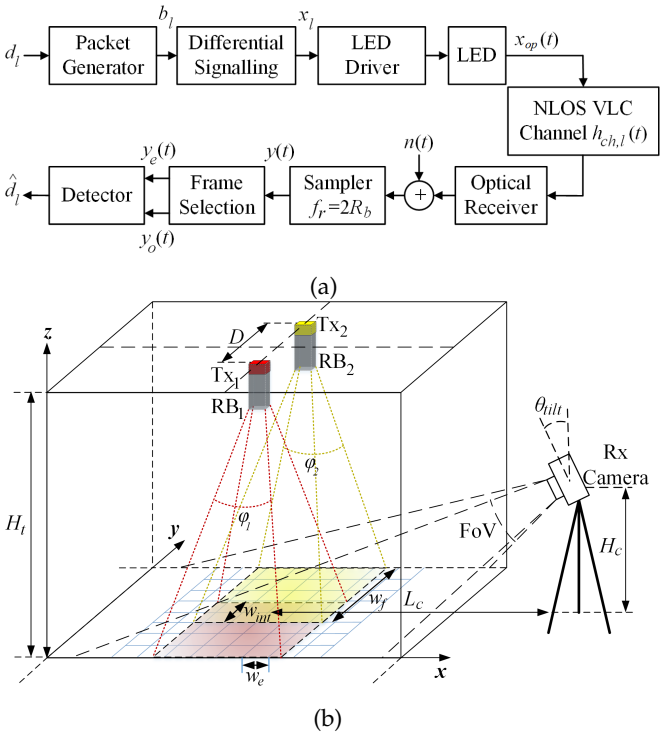


**Fig. 1.** Proposed OCC system: (a) schematic block diagram, and (b) system orientation with LEDs' illumination patterns. The camera is used to capture reflected lights.


**Fig. 2.** Proposed packet format.

parameters determine the brightness of pixels: (i) shutter speed or $T_{exp}$ - which must be smaller than $1/R_b$ in order to reduce inter-symbol interference (ISI); (ii) ISO – which determines the sensitivity of the IS; higher ISO leads to (a) increased brightness of the captured image, thereby increasing the level of perceptible shot noise (note that, noise depends primarily on the overall sensor area) [18]; and (b) a decreased dynamic range of the camera sensor; and (iii) aperture – which controls the amount of light being captured and limits or widens the depth of field. Consequently, objects located outside this range will appear hazy in the image. In non-rolling shutter-based OCC, the transmission rate is usually limited to $f_r$ (in our proposed system it is limited to half of $f_r$). For current commercial mobile phone cameras and commercial high-speed cameras' $f_r$ are $\sim$ 960 fps and > 2 Mfps, respectively.

## 3. THEORY AND SIGNAL DETECTION ALGORITHM

At the camera, assuming a linear shift-invariant model, the received optical signal $y(t)$ is given by:

$$y(t) = \mathcal{R}x_{op}(t) \otimes h(t) + n(t) + I(t), \quad \textbf{(1)}$$

where $x_{op}(t)$ is the transmitted optical signal, $h(t)$ is the combined impulse responses of the channel (NLOS) and the CMOS active pixel, $\mathcal{R}$ is the responsivity of each PD of the camera sensor, $I(t)$ is the interference from other light sources, and $n(t)$ is

the total additive white Gaussian noise [19]. Based on [20], for NLOS the transfer function of the link for the $(i,j)^{th}$ pixel of the camera is given by:

$$h_{ch,l}(i,j) = \int_{p_{i-1}}^{p_i} \int_{q_{j-1}(y)}^{q_j(y)} R_{t,l}(x,y) \frac{1}{d_{t,l}^2(x,y) d_c^2(x,y)} \times A_{pixel} R_r(x,y) \rho \cos(\psi_c(x,y)) \, \mathrm{d}A, \quad (2)$$

where $A_{pixel}$ is the effective area of each pixel, $R_{t,l}(x,y)$ and $R_r(x,y)$ are Lambertian radiation pattern of the LED and the reflection element, respectively, and $\rho$ denotes the reflection coefficient of the surface. $\mathrm{d}A = \mathrm{d}x\mathrm{d}y$ is the unit element area on the floor surface, where the intensity of incident light is assumed to be constant. $p_i$ and $q_j$ are the boundaries of the area covered by pixels in the y and x dimensions, respectively. $d_{t,l}(x,y) = \sqrt{(x-x_{t,l})^2 + (y-y_{t,l})^2 + H_t^2}$ is the distance between the Tx $(x_{t,l}, y_{t,l}, H_t)$ and the reflecting element (x,y,0), and $d_c(x,y) = \sqrt{(x-x_c)^2 + (y-y_c)^2 + H_c^2}$ is the distance between the camera $(x_c, y_c, H_c)$ and the reflecting element. The incident angle of the camera is defined as:

$$\psi_c(x,y) = \cos^{-1}(\overrightarrow{n_l}.\overrightarrow{n_c}), \quad (3)$$

where $\overrightarrow{n_l} = (x - x_c, y - y_c, -H_c)$ and $\overrightarrow{n_c} = (-\cos(\phi_{tilt})\cos(\theta_{tilt}), \sin(\phi_{tilt})\cos(\theta_{tilt}), -\sin(\theta_{tilt}))$ are the unitized incident beam and the camera plain normal vector, respectively and the dot denotes the inner product. The frequency response of the CMOS active pixel is given by [21]:

$$h_{cp}(\omega) = G e^{-j\omega T_{exp}/2} . \frac{2\sin(0.5\omega T_{exp})}{\omega}, \quad (4)$$

where $G$ is the amplification gain per pixel, and $\omega$ is the angular frequency. Note that, the 2nd and 3rd term represent the delay of $0.5T_{exp}$ between the centre of the exposure and when the sample is actually read, and the frequency response of integrating $x(t)$ over $T_{exp}$, respectively. $y(t)$ is then sampled at a sampling rate $f_r = 2R_b$, see Fig. 3, to generate a 14-bit matrix of dimensions of $(I_{raw} \times J_{raw})$ per primary colour, where $I_{raw}$ and $J_{raw}$ are the numbers of pixels of the raw image in vertical and horizontal directions, respectively. This matrix is down-sampled to generate an 8-bit matrix of size $I \times J$ per colour for the purpose of storage. Note that, the sampling duration is equal to $T_{exp}$.

In this paper, to avoid the inter-symbol interference (ISI), each bit is sampled twice to ensure that we always have a sample of the signal between the rise and fall edges. Accordingly, we define the samples in terms of two sets of odd and even samples prior to applying the detection process independently. Note that, the set with a lower BER is considered. The detailed detection process at the Rx is best illustrated by a flowchart in Fig. 4. Following selection of the odd and even frames and grayscale conversion, frame subtraction is first carried out for all odd frames followed by the even frames for the entire video frame (i.e., $I \times J$ pixels) as given by:

$$\Delta f_k = f_k - f_{k-1}, \quad (5)$$

where $f_k$ and $f_{k-1}$ are the subsequent frames. The absolute values of the mean of $\Delta f_k$ for the entire array is given by:

$$S_k = \left| \underset{i,j}{\mathrm{mean}} (\Delta f_k(i,j)) \right|, i = 1, \ldots, I, j = 1, \ldots, J, \quad (6)$$

where $I$ and $J$ are the numbers of pixels in both vertical and horizontal directions, respectively. Next, $S_k$ is compared with

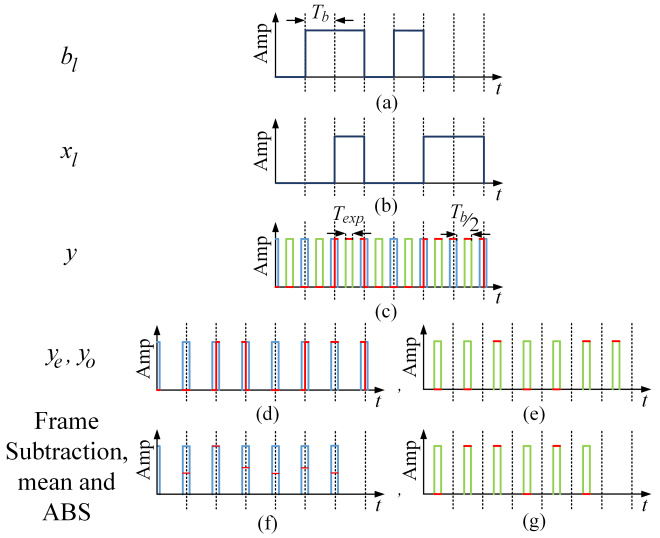


**Fig. 3.** A time frame of the system showing the procedures taking place on the input signal in each stage: (a) output of the packet generator, (b) differentially encoded data, (c) sampled data at $f_r = 2R_b$ using the camera, (d) even frames of the sampled data, (e) odd frames of the sampled data, (f) absolute value of the mean of subtracted even frames, and (g) absolute value of the mean of subtracted odd frames. Red lines show the value of the sampled data with the time.

a threshold level $th_{St}$ to regenerate the start sequence, which is then correlated with the look-up table based bit patterns of the size of $1 \times 11$. On achieving pattern matching, $Flag_{St}$ is set to 1, and a pixelated version of the mask frames is created based on averaging over blocks of $m \times n$, where $m = n =$ 10-pixel, which is given by:

$$\Delta f'_{ma,l}(i,j) = \underset{i,j}{\mathrm{mean}} (\Delta f_l(i,j)), \quad i = (\xi-1)m + 1, \ldots, \xi m, \quad j = (\zeta-1)n + 1, \ldots, \zeta n, \quad \xi = 1, \ldots, I/m, \zeta = 1, \ldots, J/n. \quad (7)$$

Accordingly, every element of $\Delta f'_{ma,l}$ is binarized to form an $I \times J$ matrix. The $(i,j)^{th}$ pixel binary value of the $l^{th}$ mask frame is given by:

$$f_{ma,l}(i,j) = \begin{cases} 1, & \Delta f'_{ma,l}(i,j) \geq th_{ma} \\ 0, & \Delta f'_{ma,l}(i,j) < th_{ma} \end{cases}, \quad l = 1, \ldots, N_{ma}, \quad i = 1, \ldots, I, \quad j = 1, \ldots, J, \quad (8)$$

where $th_{ma}$ is the threshold level for the mask.

Finally, for data recovery part of the subtracted frame is multiplied by an $I \times J$ mask matrix for $\mathrm{Tx}_l$, so that all non-illuminated pixels are set to zero as given by:

$$\boldsymbol{Z_{l,k} = \Delta f_k . f_{ma,l}}. \quad (9)$$

This procedure is performed for $N_{ma} = 2$ times in this case and then the mask stage flag, $Flag_{ma}$, is toggled to one. The mean of $\boldsymbol{Z_{l,k}}$, which is a scalar number, is given by:

$$y_{l,k} = \underset{i,j}{\mathrm{mean}} (Z_{l,k}(i,j)). \quad (10)$$

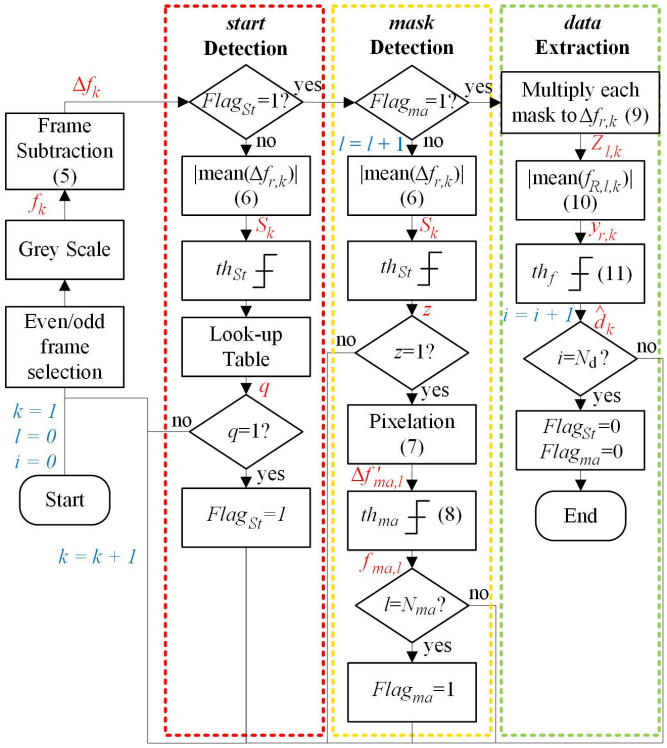


**Fig. 4.** A flowchart illustrating the detection process to recover the data.

$y_{l,k}$ is then compared with a threshold level $th_f$ to regenerated the transmitted data stream as given by:

$$\hat{d}_{l,k} = \begin{cases} 1, & y_{l,k} \geq th_f \\ 0, & y_{l,k} < th_f \end{cases}. \tag{11}$$

## 4. EXPERIMENTAL RESULTS

Fig. 5 shows the experimental setup for evaluation of the proposed system. A TTi TGA12104 arbitrary waveform generator was used to generate a pseudo random NRZ-OOK pattern of length 1000 bits. Two identical light sources each composed an array of 48-LEDs (chip-on-board COB LEDs) mounted on a heat sink were placed within the tent at a hight of 1.8 m and a distance of 1 m from each other. The illumination profiles of the light sources are similar to the Lambertian emission pattern of $E(\theta) = \frac{(m+1)}{2}\cos^m(\theta)$ where $m = 1$ and $2/3$ in horizontal and vertical directions, respectively, and have linear optical power-current characteristics with a wide current dynamic range of 300 mA. The floor surface was covered by sheets of white paper. Fig. 6(a) shows the light source's normalized illumination footprint on the floor plane, which was measured using an optical power meter. Note that, the illumination level of diffracted light from the edges of rectangular boxes are about 10% of the maximum illuminance level of the light source. The floor surface area of 120 × 120 cm was divided into a number of segments of size of 3×3 cm, and the normalized measured reflection pattern of light reflected from each segment at a distance of 50 cm in the polar plot is depicted in Fig. 6(b), which matches with the normalized 1st order Lambertian emission pattern. We observed the same profile in every segments.

A camera (Canon Rebel SL1 EOS 100D) was used to capture

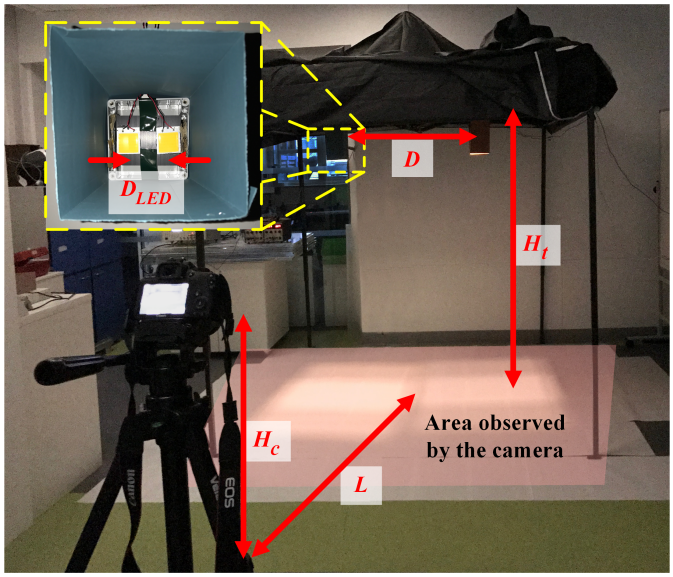


**Fig. 5.** Experimental setup for the proposed system and the light source shown in the inset. The floor surface is covered by sheets of white paper and the red-highlighted area is the area that the camera observes.

**Table 1. System Parameters**

| Symbol | Description | Value |
|---|---|---|
| $H_t$ | Height of the Tx | 1.8 m |
| $D$ | Distance between two Txs | 1 m |
| $N_{data}$ | Number of payload data bits | 1000 bits |
| $N_{mask}$ | Number of mask bits | 3 bits |
| $N_{start}$ | Number of start bits | 11 bits |
| $D_{LED}$ | Distance between two COB-LED | 6 cm |
| $R_b$ | Transmitter bit rate | 30 bps |
| $L$ | Link ground span | 3 m |
| $\rho$ | Reflection coefficient of the floor | 0.13 |
| $H_c$ | Height of the camera | 1.3 m |
| $f_r$ | Camera frame rate | 60 fps |
| $\theta_{tilt}$ | Tilt angle | $20^o$ |
| $f$ | Camera focal length | 18 mm |
| $L_{RB}$ | Length of the box | 28 cm |
| $A_{pixel}$ | Pixel area | 18.4 $\mu$m$^2$ |
| $A_{IS}$ | Image sensor area | 22.3×14.9 mm |
| $I_{raw} \times J_{raw}$ | Camera raw image Resolution | 5184×3456 |
| $I \times J$ | Resolution of saved frames | 1280×720 |

a 5.8 minutes long video stream at the RGB-coloured HD resolution (i.e.,1280×720), and at 60 fps. The captured video was then processed off-line in the Matlab domain, where subtracted frames were pixelated over blocks of 10×10 pixels in order to detect the mask. By this approach, we achieved 100 times reduction in the noise variance, thus leading to clearer mask. All the key system parameters are shown in Table I.

Fig. 7 shows the measured BER as a function of the transmit power for different values of ISO, an aperture of $f4$, a shutter speed of 1/100 s, a link span of 5 m between the camera and the transmitter via a NLOS path, and a camera tilt angle of

$20^o$. Since in this work, we have adopted averaging over the area we observe improved BER performance at higher ISOs. For example, at a BER of $10^{-3}$ (i.e., the forward error correction (FEC) limit) the power penalties are 3 and 6 dB for ISOs 3200 and 1600, respectively compared to ISO 6400. This is because ISO 6400 implies doubling the pre-amplification gain compared to ISO 3200, and pixel averaging, which reduces the effect of ISO on the intensity variance. The same trend in the BER performance is also observed for a range of camera aperture of $f4$, $f5.6$, and $f8$ and $T_{exp} = 1/100$.

Next, we considered $T_{exp}$ of the camera for a given ISO and under the focused condition. Fig. 8 depicts the BER against the transmit power for a range of $T_{exp}$ (i.e., 1/100, 1/200, 1/400 and 1/800 s) and for an aperture of $f4$. At a BER of $10^{-3}$ we observe a 3 dB power penalty for every doubling of $T_{exp}$ toward $T_{exp}$ of 1/100. Note that, increasing and decreasing $T_{exp}$ can lead to a higher chance of capturing the rise and fall time edges of OOK-NRZ and decreasing the exposure level of the recorded image, respectively.

To find the impact of interference from other sources, we used the following parameters for the camera $T_{exp}$ = 1/100 ms, aperture of f3.5 and ISO of 6400. Here, we define the intersection ratio $r_{int} = w_{int}/w_f$ , where $w_{int}$ and $w_f$ denote the width of intersecting and the footprint area, respectively. We set the transmit power $P_t$ to 20 dBm per the Tx. Fig. 9 shows the BER performance of the proposed link as a function of $r_{int}$. Note that,

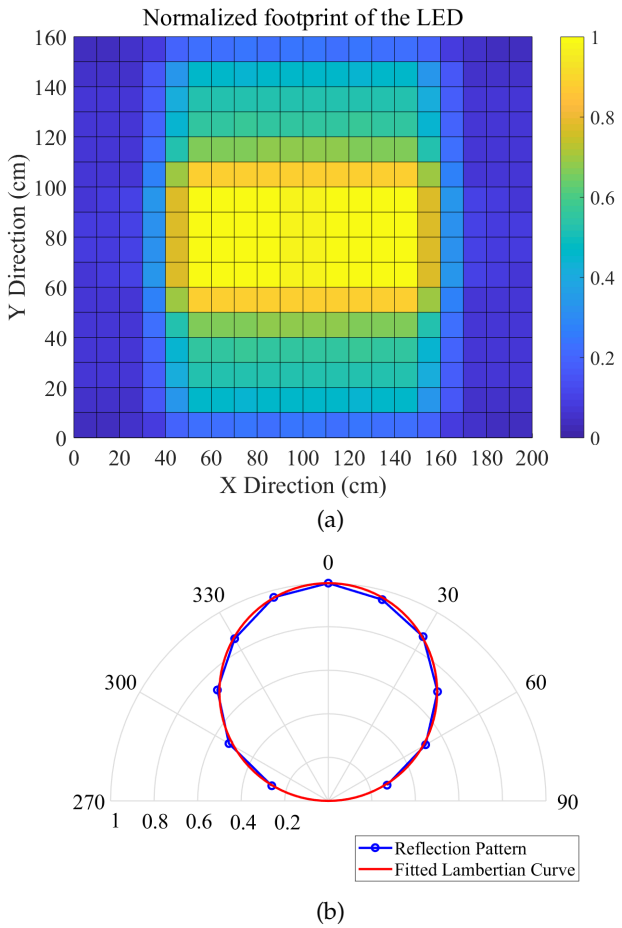


**Fig. 6.** Normalized: (a) footprint of the LED on the floor plane, and (b) reflection beam profile.

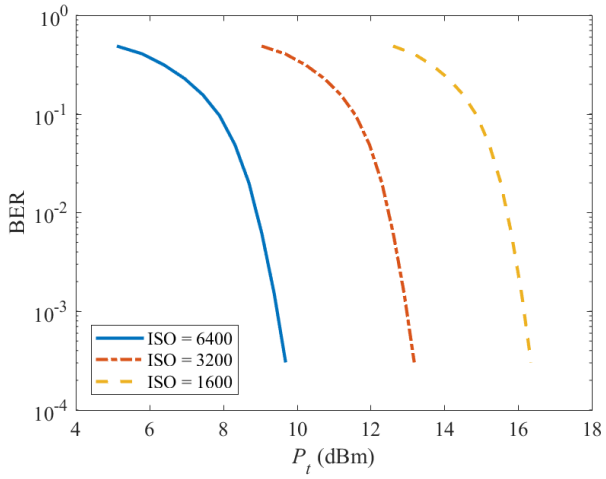


**Fig. 7.** BER vs. the transmit power for different values of ISO, an aperture of $f4$, a link span of 5 m, and an exposure time of 1/100 s in the focused mode.

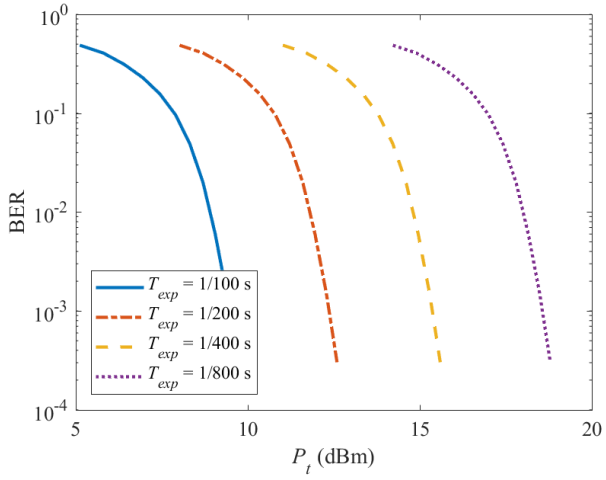


**Fig. 8.** BER vs. the transmit power for different exposure times, an aperture of $f4$, a link span of 5 m, and ISO of 6400 in the focused mode.

for $r_{int} > 0.3$, the BER is higher than the FEC limit, and therefore a reliable link cannot be established.

## 5. CONCLUSION

We have reported for the first time a novel $2 \times N$ indoor OCC system, which extracts the data information from the non-line-of-sight beams. We proposed a dedicated packet structure and a detection methodology for extracting the data from the recorded video streams. An experimental test bed was developed for the proposed system. We showed that higher ISO levels and exposure times led to a reduced transmit power level by up to 6 dB for ISO of 6400 compared to ISO of 1600, and 3 dB for every doubling of the exposure time at a BER of $10^{-3}$. We also showed that the proposed system works well for the intersection ratio lower than 0.3.

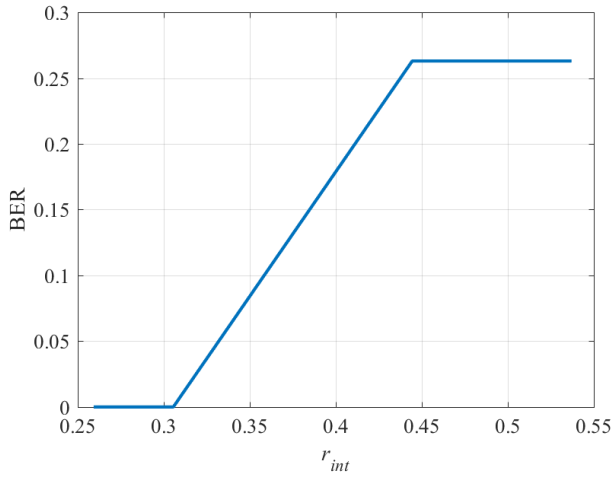


**Fig. 9.** BER vs. width of intersection ratio , rint when two transmitters are 1 m apart for ISO of 6400, aperture of $f3.5$, exposure time of $1/100$ s and $P_t = 20$ dBm.

**Funding.** Engineering and Physical Sciences Research Council (EPSRC)(EP/P006280/1) and Grantová Agentura České Republiky (GACR) (17-17538S).

## REFERENCES

1. Z. Ghassemlooy, L. N. Alves, S. Zvanovec, and M.-A. Khalighi, *Visible Light Communications: Theory and Applications* (CRC Press, 2017).
2. A. Burton, H. Minh, Z. Ghassemlooy, E. Bentley, and C. Botella, "Experimental demonstration of 50-mb/s visible light communications using 4× 4 mimo," IEEE Photonics Technology Letters **26**, 945–948 (2014).
3. S. Hranilovic and F. R. Kschischang, "Short-range wireless optical communication using pixilated transmitters and imaging receivers," in "Communications, 2004 IEEE International Conference on," , vol. 2 (IEEE, 2004), vol. 2, pp. 891–895.
4. P. Luo, M. Zhang, Z. Ghassemlooy, H. Le Minh, H.-M. Tsai, X. Tang, and D. Han, "Experimental demonstration of a 1024-qam optical camera communication system," IEEE Photonics Technology Letters **28**, 139–142 (2016).
5. C. Danakis, M. Afgani, G. Povey, I. Underwood, and H. Haas, "Using a cmos camera sensor for visible light communication," in "Globecom Workshops (GC Wkshps), 2012 IEEE," (IEEE, 2012), pp. 1244–1248.
6. P. H. Pathak, X. Feng, P. Hu, and P. Mohapatra, "Visible light communication, networking, and sensing: A survey, potential and challenges," ieee communications surveys & tutorials **17**, 2047–2077 (2015).
7. I. Takai, S. Ito, K. Yasutomi, K. Kagawa, M. Andoh, and S. Kawahito, "Led and cmos image sensor based optical wireless communication system for automotive applications," IEEE Photonics Journal **5**, 6801418–6801418 (2013).
8. Sony, "Sony xperia xz premium," https://www.sonymobile.com/gb/products/phones/xperia-xz-premium/specifications.
9. T. Nagura, T. Yamazato, M. Katayama, T. Yendo, T. Fujii, and H. Okada, "Tracking an led array transmitter for visible light communications in the driving situation," in "Wireless Communication Systems (ISWCS), 2010 7th International Symposium on," (IEEE, 2010), pp. 765–769.
10. R. Boubezari, H. Le Minh, Z. Ghassemlooy, and A. Bouridane, "Novel detection technique for smartphone to smartphone visible light communications," in "Communication Systems, Networks and Digital Signal Processing (CSNDSP), 2016 10th International Symposium on," (IEEE, 2016), pp. 1–5.
11. Y. Kawai, T. Yamazato, H. Okada, T. Fujii, T. Yendo, S. Arai, and K. Kamakura, "Tracking of led headlights considering nlos for an image sensor based v2i-vlc," in "International Conference and Exhibition on Visible Light Communications," (2015).
12. S. Arai, Y. Shiraki, T. Yamazato, H. Okada, T. Fujii, and T. Yendo, "Multiple led arrays acquisition for image-sensor-based i2v-vlc using block matching," in "Consumer Communications and Networking Conference (CCNC), 2014 IEEE 11th," (IEEE, 2014), pp. 605–610.
13. H. Chinthaka, N. Premachandra, T. Yendo, T. Yamasato, T. Fujii, M. Tanimoto, and Y. Kimura, "Detection of led traffic light by image processing for visible light communication system," in "Intelligent Vehicles Symposium, 2009 IEEE," (IEEE, 2009), pp. 179–184.
14. S. Teli, W. A. Cahyadi, and Y. H. Chung, "Optical camera communication: Motion over camera," IEEE Communications Magazine **55**, 156–162 (2017).
15. W.-C. Wang, C.-W. Chow, L.-Y. Wei, Y. Liu, and C.-H. Yeh, "Long distance non-line-of-sight (nlos) visible light signal detection based on rolling-shutter-patterning of mobile-phone camera," Optics Express **25**, 10103–10108 (2017).
16. N. Rajagopal, P. Lazik, and A. Rowe, "Visual light landmarks for mobile devices," in "Proceedings of the 13th international symposium on Information processing in sensor networks," (IEEE Press, 2014), pp. 249–260.
17. T. Yamazato, I. Takai, H. Okada, T. Fujii, T. Yendo, S. Arai, M. Andoh, T. Harada, K. Yasutomi, K. Kagawa *et al.*, "Image-sensor-based visible light communication for automotive applications," IEEE Communications Magazine **52**, 88–97 (2014).
18. J. Schewe, *The digital negative: raw image processing in Lightroom, Camera Raw, and Photoshop* (Peachpit Press, 2015).
19. H. J. Trussell and M. J. Vrhel, *Fundamentals of digital imaging* (Cambridge University Press, 2008).
20. J. M. Kahn and J. R. Barry, "Wireless infrared communications," Proceedings of the IEEE **85**, 265–298 (1997).
21. J. C. Chau and T. D. Little, "Analysis of cmos active pixel sensors as linear shift-invariant receivers," in "Communication Workshop (ICCW), 2015 IEEE International Conference on," (IEEE, 2015), pp. 1398–1403.